

# A HIGH-FIDELITY MDO FRAMEWORK APPLIED TO THE DESIGN OF A HIGH ASPECT-RATIO TRANSPORT WING

L. Martins-Pacheco<sup>\*†</sup>, Ö. Petersson<sup>\*</sup>, A. C. Marta<sup>†</sup>, F. Volle<sup>‡</sup>

<sup>\*</sup> Airbus Defence and Space GmbH, Department of Stress Methods and Optimisation, Rechliner Straße, 85077, Manching, Germany

<sup>†</sup> IDMEC, Instituto Superior Técnico, Universidade de Lisboa, Av. Rovisco Pais, 1, 1049-001 Lisboa, Portugal

<sup>‡</sup> DLR (German Aerospace Center), Institute of Aerodynamics and Flow Technology, Lilienthalplatz 7, 38108, Braunschweig, Germany

## Abstract

A high-fidelity multidisciplinary design optimisation (MDO) framework was applied to the structural sizing and performance evaluation of high-aspect-ratio transport wings. Using Airbus Defence and Space's MDO suite, Lagrange, two aircraft models based on the DLR F25, one with an aspect ratio of 15.5 and the other 17.4, were structurally sized through gradient-based methods. These optimisations considered the composite wing covers and spars as sizing parameters, and were subject to strength, buckling and manufacturing constraints. Following the structural sizing, performance prediction analysis for both aircraft were conducted using a high-fidelity MDO framework, which couples Lagrange with DLR's TAU within FlowSimulator. The aim of this study was to explore the aero-structural trade-offs resulting from an increased aspect ratio. The results show that both aspect ratios exhibited similar trends in skin thickness distribution, ply share allocation, and spar and stringer sizing. However, the higher aspect ratio wing, despite experiencing a 5.51% increase in wing structural mass, demonstrated a 1.47% improvement in Breguet range, primarily due to its reduced induced drag and increased lift generation. The findings highlight the potential of high-aspect-ratio wings to enhance overall performance, albeit at the expense of increased structural weight.

## Keywords

Multidisciplinary Design Optimisation; MDO; Structural Sizing; High-Fidelity Performance Analysis

## 1. INTRODUCTION

The aviation industry faces a paramount challenge of achieving sustainability in the forthcoming decades. As global priorities shift towards ambitious climate objectives, the sector must rapidly adapt to align with these environmental goals. Central to this transformation is a significant enhancement in overall efficiency, spanning both aerodynamic and structural aspects.

A key avenue for improving aerodynamic efficiency lies in the use of high aspect-ratio wings. However, these designs typically lead to increased structural mass. Addressing this trade-off requires the implementation of Multidisciplinary Design Optimization (MDO) techniques, which are essential for exploring the intricate design space and determining the optimal balance between aerodynamic performance and structural integrity.

MDO makes it possible to incorporate the interactions between multiple disciplines, such as aerodynamics and structures, into the evaluation process and allow for an efficient exploration of complex trade-offs while adhering to extensive competing constraints from various engineering disciplines.

In the present work, Airbus Defence and Space's MDO suite Lagrange [1] is employed to structurally size two high-aspect-ratio wing aircraft. The first aircraft is the

DLR F25 model with an Aspect Ratio (AR) of 15.5, while the second is a modified version of the DLR F25, featuring an increased span and area, resulting in an AR of 17.4. The optimisation considers two load cases, as well as two different mass configurations per aircraft, and incorporates sizing parameters for the composite wing covers and spars. These parameters are optimised under strict strength, buckling, and manufacturing constraints, aiming to reflect industry requirements with appropriate simplicity.

Once the structural sizing of both aircraft models is completed, a quantitative comparison of their performance will be conducted to assess the impact of the increased aspect ratio on lift distribution, drag, and range. To evaluate these performance metrics, a high-fidelity MDO framework will be employed.

## 2. PROBLEM FORMULATION

With the goal of improving performance, the engineering design problem can be formulated as a mathematical optimisation problem as follows:

$$\begin{aligned}
(1) \quad & \min_z F(z, y) \\
& \text{subject to } C(z, y) \geq 0 \\
& y = Y(z) \\
& z_{\text{lower}} \leq z \leq z_{\text{upper}}.
\end{aligned}$$

In this formulation, the objective function  $F$  represents the performance metric to be optimised, and the criteria model  $C$  includes all constraints that must be satisfied to achieve a feasible design. To accurately predict the performance metric and constraints, an analysis model is employed to determine the state variables  $y$  by solving the governing equations  $Y$ . The vector  $z$  represents the design variables, which influence both the objective function  $F$  and the constraint model  $C$  through the state variables  $y$ . These design variables can encompass parameters related to shape and size and are subject to both upper and lower bounds.

## 2.1. Objective

The objective of the optimisation is to minimise (or maximise) a performance metric  $F(z, y)$ , which represents a balance across multiple interdependent engineering disciplines. By appropriately defining this objective, the optimisation algorithm can effectively manage trade-offs between various factors, such as reducing aerodynamic induced drag whilst ensuring structural soundness.

## 2.2. Criteria Model

A robust criteria model is essential to prevent optimisations from converging on impractical or infeasible solutions. In the context of aircraft design, criteria related to structural sizing are particularly important. These criteria ensure that the airframe is sufficiently robust to withstand the various loads experienced during flight, thereby avoiding potential structural failures.

Structural integrity criteria are crucial not only for ensuring safety and regulatory compliance but also for the overall performance optimisation. Structural sizing directly impacts the aircraft's weight, which, in turn, affects fuel efficiency and handling. Furthermore, the size and stiffness of the wing structure significantly influence the aircraft's aerodynamic performance. For instance, the in-flight shape of the aircraft wing, especially those with high-aspect-ratios, is affected by its structural properties through aeroelastic effects. Adequately addressing these criteria ensures a balance between structural strength, weight, and stiffness, leading to a more effective and efficient design.

## 2.3. Optimisation Algorithm

Selecting an appropriate optimisation algorithm is crucial for tackling a multi-disciplinary optimisation problem. Given the complexity of aircraft optimisation models, which involve numerous design variables and intensive computational evaluations, gradient-based optimisation methods are often preferred. These algorithms utilise local gradient information to update the design variables

at each iteration. To achieve this, an efficient sensitivity analysis of both the objective function and constraints with respect to the design variables is essential for ensuring both accuracy and computational efficiency.

## 2.4. Analysis Models

In the present work, to ensure the structural safety of the aircraft across the flight envelope, a low-fidelity aerodynamics solver is coupled with a high-fidelity structural solver for structural sizing. Conversely, to accurately determine the performance of the sized aircraft, a high-fidelity fluid flow solver is coupled with the same structural solver. It is important to note that the operating conditions driving the structural sizing process are typically not relevant to the aircraft's performance assessment, and vice versa.

To perform structural sizing in a cost-efficient manner, while accounting for aeroelastic interactions between the structural mechanics and aerodynamics of the wing, a lower-fidelity fluid flow model based on linear aerodynamics is employed to calculate aeroelastic loads at the structurally critical design points. Aircraft sizing, following industry standards, such as those used by Airbus Defence and Space, considers a high number of loading conditions and constraints. Consequently, the use of high-fidelity computational fluid dynamics (CFD) models, which significantly increase the computational cost of evaluating solutions and their gradients, becomes prohibitive. Additionally the high fidelity fluid flow models are not very robust for the high wing tip displacements imposed by the structurally critical loads needed for sizing.

The high-fidelity aero-structural analysis is reserved for accurately predicting the performance of the already sized aircraft. High-fidelity CFD is necessary for this stage, as accurate predictions of aerodynamic drag, which cannot be obtained with lower-fidelity models, are crucial for aircraft performance determination.

## 3. IMPLEMENTATION

In the present study, the aircraft models are initially sized using the MDO suite Lagrange to ensure the required levels of structural integrity. Subsequently, the performance of the sized aircraft will be assessed using DLR's FlowSimulator environment [2].

### 3.1. Structural Integrity

For the structural sizing optimisation, Airbus Defence and Space's MDO suite Lagrange is employed. This MDO tool incorporates a range of gradient-based optimisation algorithms and allows for the use of both shape (element geometry) and sizing (element thickness) variables, allowing for various types of constraints including strength, buckling, and manufacturing. Lagrange facilitates the structural sizing process by handling a large number of subcases and multiple mass configurations simultaneously.

### 3.1.1. Aero-Structural Analysis

Lagrange's built-in finite element solver is coupled with a low-fidelity Doublet Lattice Method (DLM) linear aerodynamics model. For aeroelastic analysis, to compute the aerodynamic loads acting on the structure, Lagrange is able to read an Aerodynamic Influence Coefficient (AIC) matrix. In both aerodynamic and structural analysis, the generation of models and meshes follows different criteria. Specifically, the meshes at the fluid-structure interface differ, and because parameters such as structural deflection or aerodynamic loads are defined at different grid nodes, direct information exchange is not feasible. To facilitate the transfer of displacement and load information between the aerodynamic and structural domains, a set of splines is defined for interpolation.

Throughout the structural sizing process, feasible trim states of the aircraft are determined using Lagrange's optimisation capabilities. This ensures that the aerodynamic loads used for structural sizing remain accurate and reflective of the actual flight conditions.

### 3.1.2. Structural Sizing Requirements

The structural sizing requirements for composite wings focus primarily on optimising the wing covers, as they are the main drivers of composite wing aeroelastic tailoring, including both passive load alleviation and improvements in cruise drag performance.

To achieve a composite wing sizing that yields a manufacturable wing with realistic weight and stiffness, strength, buckling, and minimum thickness requirements need to be applied as constraints in Lagrange.

### 3.1.3. Strength Requirements

Industrial strength requirements for typical composite wing sizing consider a range of failure modes, each with specific checks using distinct analysis tools. To simplify the strength sizing process, a maximum tension and compression material strain allowable is considered for each component as a requirement for wing sizing. A conservative approach was adopted, using the most restrictive material allowable for the most critical strength driver recommended.

### 3.1.4. Buckling Requirements

Buckling requirements for composite wing sizing mandate that the wing covers must not experience buckling below the limit load. To prevent buckling from becoming a significant design driver, a minimum stringer and rib pitch was implemented during the design. For simplification in the buckling requirements, the skin panels are modelled as bi-axially loaded, simply supported flat plates with anisotropic material properties. The critical buckling loads on these skin panels were determined using the methods proposed by P.M. Weaver [3, 4]. For stringer buckling analysis, both the stringer and the attached sheets were treated as a super stiffener. The critical buckling strength of the combined super stiffener is determined using the Johnson-Euler formula [5].

### 3.1.5. Minimum Thickness Requirements

Different minimum laminate thicknesses are used for skin sizing in various areas of the wing to represent specific requirements. For instance, in the upper skin, lightning strike protection imposes a certain minimum thickness, while in the lower skin, different minimum thicknesses are applied due to risks such as wheel and tyre debris impact, or in the vicinity of the engine where increased thickness is required for bolted joints in the pylon attachment area. For a more realistic sizing, variations in skin thickness should also be limited, with ramp rate requirements applied for skin thickness in both span and chord directions. Additionally, a minimum thickness must be applied to the foot and web of the stringers due to manufacturing constraints.

### 3.1.6. Ply Share Requirements

The composite skin laminates will have variable ply shares, which can be adjusted in the optimisation as long as certain rules regarding maximum and minimum ply share percentages are followed. A continuity requirement between the thickness of plies of adjacent skin patches ensures manufacturability of the wing. The spars will have fixed ply share percentages along their length with a predefined laminate definition.

### 3.1.7. Maximum Wing Tip Twist

The maximum wing tip twist during cruise will be restricted to prevent issues such as excessive stress on the root or fatigue damage.

## 3.2. Flight Performance

To evaluate the performance of the sized aircraft, a recently developed high-fidelity Multidisciplinary Design Optimization framework [6, 7] is employed.

This analysis utilises a three-field formulation of the coupled aero-structural problem, in which mesh deformation is added as a discipline alongside the aerodynamic and structural disciplines.

In this formulation, the residuals  $R \equiv \{R_F, R_M, R_S\}$  represent the discretised governing equations for flow analysis, mesh deformation, and structural analysis, respectively. The state variables are defined as  $y \equiv \{y_F, y_M, y_S\}$ , where  $y_F$  denotes the fluid state within the computational fluid dynamics mesh,  $y_M$  represents the volume mesh coordinates to be deformed, and  $y_S$  refers to the structural displacements.

### 3.2.1. Aerodynamic Discipline

The fluid flow is governed by the Reynolds-averaged Navier-Stokes (RANS) equations with the Spalart-Allmaras (SA-neg) one-equation turbulence model. In differential form, the governing equation is

$$R_F = \frac{\partial y_F}{\partial t} + \nabla \cdot (\phi_c - \phi_v) = 0,$$

where  $R_F$  is the fluid flow residual,  $\phi_c$  and  $\phi_v$  are the convective and diffusive terms, respectively the state vari-

ables  $y_F$  represent the conserved quantities of the flow, i.e., density, momentum, and total energy. These variables depend on the mesh state  $y_M$ . The equations are discretised using the Finite Volume Method (FVM) and are solved using the DLR’s high-fidelity fluid flow solver TAU [8, 9].

### 3.2.2. Structural Discipline

The structural problem is governed by the equations of linear elasticity. By applying the finite-element method (FEM) for discretisation, the structural residual  $R_S$  is expressed as

$$R_S = Ky_S - F_S = 0,$$

where  $K$  is the symmetric stiffness matrix,  $y_S$  is the state vector representing the structural displacements, and  $F_S$  is the sum of the aerodynamic and inertial forces acting on the structure. The built-in finite element solver of Airbus’s MDO suite Lagrange is used to solve the structural problem.

### 3.2.3. Loads and Displacement Transfer

The aero-structural coupled system is solved iteratively by sequentially updating the solutions for fluid flow, structural, and the fluid mesh sub-problems. The aero-structural coupling is performed using the Moving Least Squares (MLS) method [10] to map and transfer the forces and displacements at the interface of the structural and aerodynamic boundary meshes.

At each iteration, the forces on the aerodynamic mesh boundary are integrated from the flow solution  $y_F$  and transferred as boundary conditions to the structural mesh boundary, yielding the aerodynamic forces on the structural nodes. Similarly, the structural displacements at the fluid-solid interface of the finite-element mesh, a subset of the new structural state  $y_S$ , are transferred back onto the corresponding surface of the fluid mesh. These displacements serve as boundary conditions in the volume mesh deformation sub-problem and are used in the mesh deformation analysis to update the coordinates of the mesh points in the fluid domain for the next iteration.

### 3.2.4. Aerodynamic Mesh Deformation

The aerodynamic analysis requires a mesh that adapts to the structural deformation. The mesh deformation method employed on the used framework is based on the linear elasticity analogy by Rempke [11]. The governing equation of the method is

$$R_M = K_M y_M - f_M(u) = 0,$$

where  $R_M$  is the mesh deformation residual,  $K_M$  is a symmetric matrix constructed by assigning a stiffness to each element of the fluid flow volumetric mesh, inversely proportional to the element’s volume and  $f_M$  is a fictitious force that enforces the Dirichlet boundary condition of structural displacements interpolated on the aerodynamic surface mesh.

### 3.2.5. Aero-Structural Analysis

For the aero-structural analysis for performance, DLR’s FlowSimulator, an environment designed for multidisciplinary applications on high-performance computing (HPC) platforms that integrates both TAU and Lagrange solvers, is used. The mesh deformation and mapping methods utilised in this work are also available in this environment.

The aero-structure coupling is essential for capturing the effects of aeroelasticity on the in-flight wing shape deformation and its impact on performance. This coupling is addressed through an iterative solution process, which sequentially solves the fluid flow, load transfer, structural deformation, displacement transfer, and aerodynamic mesh deformation problems. The coupling process begins with TAU solving the RANS-SA fluid flow equations, as detailed in Section 3.2.1. Following this, using the load interpolation approach described in Section 3.2.3, the aerodynamic loads at the fluid-structure interface are interpolated onto the structural mesh nodes. Taking these aerodynamic forces and inertia loads into account, Lagrange’s finite element solver computes the structural deformations, as outlined in Section 3.2.2. The resulting structural deformations are then transferred as displacements onto the aerodynamic mesh surface, where they are applied as boundary conditions in the mesh deformation problem of the aerodynamic volume mesh, described in Section 3.2.4. This process is repeated until convergence is achieved.

Aircraft trimming is crucial for accurately determining performance. To simulate free-flight conditions, the aero-structural coupling is embedded within a gradient-based trimming process, which balances the inertial and aerodynamic forces. The trimming variables employed in this study are the angle of attack and elevator.

## 4. TEST CASE - DLR F25

In this work, the DLR F25 model is used as a baseline for the test case. The F25 is a short- to medium-range, narrow-body aircraft with a high-aspect-ratio wing of 15.5. Based on this baseline, a new aircraft model is generated by increasing the span and area of the wing to achieve a higher aspect ratio of 17.4. These two aircraft models will be referred to as F25-AR15 and F25-AR17, respectively. Although it is possible to increase the aspect ratio while keeping the wing area constant, this study focuses on increasing the span of the wing sections outboard of the pylon area to maintain the original pylon attachment configuration. In Table 1, the main geometrical differences between the F25-AR15 and F25-AR17 wings are presented.

	F25-AR15	F25-AR17
Aspect Ratio	15,50	17,44
Span [m]	44,60	49,04
Area [m <sup>2</sup> ]	129,59	139,21

TAB 1. Geometric comparison between F25-AR15 and F25-AR17 configurations.

#### 4.1. Structural Model

Both aircraft structural models were generated using Airbus Defence and Space's in-house tool Descartes [12]. The skins, spars, and ribs are modelled using shell elements, while the stringers and spar caps are represented by either rod or beam elements. The engine and pylon are treated as point masses, with their connection to the wing and engine modelled using rigid body elements. Table 2 provides a summary of the structural elements used in each model.

	F25-AR15	F25-AR17
Nodes	13,152	13,331
Shell Elements	14,758	19,721
Rod Elements	5,812	5,906
Beam Elements	3,175	3,331

TAB 2. Comparison of structural elements between F25-AR15 and F25-AR17.

The structural model for the F25-AR15 is shown in Figure 1, with the F25-AR17 constructed using the same approach.

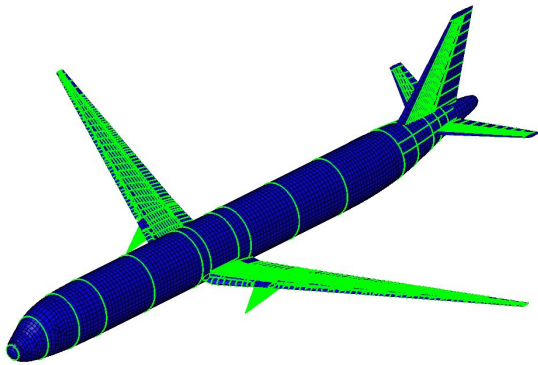


FIG 1. F25-AR15 Structural Model.

Two mass configurations were considered: the maximum take-off weight,  $MTOW = 81,656$  kg, and the maximum zero fuel weight,  $MZFW = 69,322$  kg. The mass models of the aircraft are split into two components: the structural weight of the composite wing, determined by the sizing and material properties, and concentrated masses representing the rest of the aircraft structure, systems, fuel, payload, and passengers.

The composite wing skin is modelled using a generic balanced 24-ply carbon fibre reinforced polymer (CFRP) with four ply directions ( $0^\circ$ ,  $90^\circ$ , and  $\pm 45^\circ$ ), and a density of  $1580$  kg/m<sup>3</sup>. For the spar webs, a similar 20-ply generic CFRP was used. The T-shaped stringers and spar caps are modelled with generic homogenized CFRP properties, with a density of  $1750$  kg/m<sup>3</sup>.

#### 4.2. Aerodynamic Models

##### 4.2.1. Structural Sizing

As mentioned in Section 3.1.1, the Doublet Lattice Method is used to estimate the aerodynamic loads for structural sizing. Figure 2 shows the panel model for the F25-AR15. For the F25-AR17, the panel model is adjusted to account for the new platform.

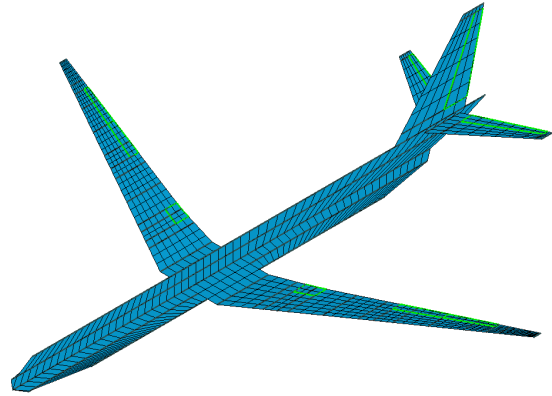


FIG 2. F25-AR15 Aerodynamic Doublet Lattice Method Panel Model.

##### 4.2.2. Flight Performance

The high-fidelity aerodynamic performance is evaluated by solving the Reynolds-Averaged Navier-Stokes (RANS) equations at cruise conditions. For the performance analysis, the aerodynamic model for both aircraft configurations is based on a conventional wing and tube layout. As the aircraft are symmetrical, half models are used for computational efficiency. For the F25-AR15, the computational grid consists of 1.02 million nodes. The aircraft is trimmed to inertial weight at a Mach number of 0.78 and an altitude of 10,363 m, with a Reynolds number of 22 million. The high-fidelity aerodynamic model for the F25-AR17 is topologically identical to that of the F25-AR15. Figure 3 illustrates the aerodynamic mesh used for the performance evaluation of the F25-AR15.

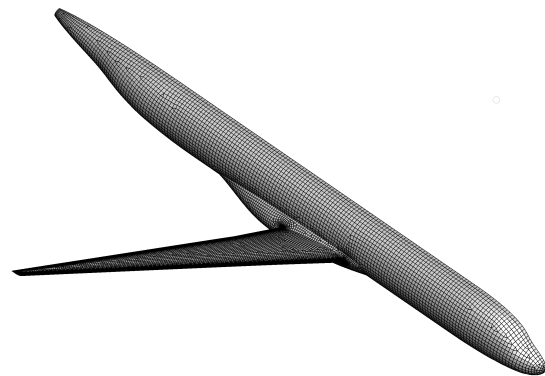


FIG 3. F25-AR15 High-Fidelity Aerodynamic Mesh For Performance Analysis.

### 4.3. Aero-Structural Coupling Models

Aeroelastic analysis requires a coupling scheme between aerodynamics and structural mechanics to enable the transfer of forces and displacements.

For the structural sizing, the aerodynamic panels shown in Figure 2 are coupled with the stiffness model shown in Figure 1 using splines. The aerodynamic forces are splined to nodes strategically placed throughout the wing box, leading and trailing edge devices, fuselage, and horizontal and vertical tailplanes. These nodes are rigidly linked to the structure. Figure 4 illustrates the splining for the F25-AR15 wing. Adjustments are made for the F25-AR17 due to its larger span.

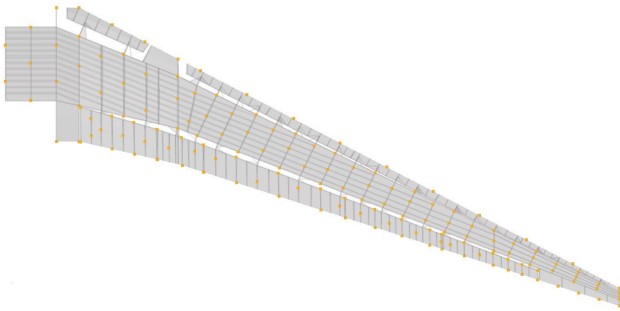


FIG 4. F25-AR15 Wing Splining For Coupling.

For the high-fidelity performance analysis, a the MLS coupling model is used, as described in Section 3.2.3.

### 4.4. Optimisation Problem

The objective of the structural sizing of the F25 is to minimize the structural weight. The NLPQL algorithm [13] is used for this optimisation, and the problem converges according to a Karush-Kuhn-Tucker (KKT) criterion [14] of  $1 \times 10^{-5}$ .

The aircraft models are sized for a 2.5g pull-up manoeuvre and a -1g push-over manoeuvre, considering both of the aforementioned mass configurations.

The wing's design variables are grouped into patches and are symmetrically linked. In the wing skin, each patch is defined by two ribs and two stringers, see Figure 5, while stringers and spar are segmented by the ribs. In each skin and spar web patch, three design variables control the thickness of the generic ply directions. The  $0^\circ$  and  $90^\circ$  layers are independently controlled, while the  $\pm 45^\circ$  layers are linked to ensure manufacturability. In the 1D segments, one to four design variables control the dimensions or cross-sectional areas.

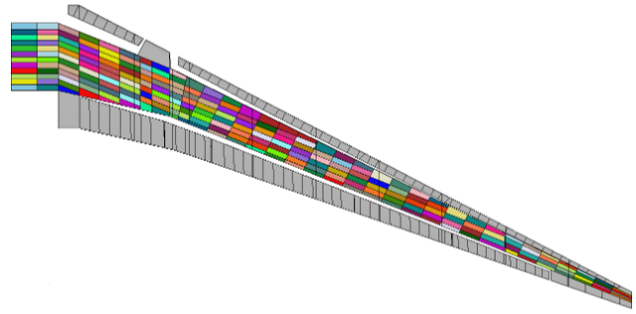


FIG 5. F25-AR15 Upper Skin Design Variables

Constraints are applied based on simplified industry standards, as discussed in the requirements for structural sizing in Section 3.1. Strength constraints are universally enforced, with allowable tension and compression strains set to  $5000 \mu\epsilon$  and  $-3500 \mu\epsilon$ , respectively, and a safety factor of 1.5 imposed. Buckling constraints are applied across the same patches used for defining the design variables.

Manufacturing constraints include a minimum upper skin thickness of 4 mm. In the lower skin, a minimum thickness of 20 mm is imposed in the pylon attachment area, with 6 mm and 8 mm minimum thicknesses applied outboard and inboard of this region, respectively. Ramp rates of 1:20 spanwise and 1:10 chordwise are enforced to limit thickness variation, along with continuity constraints between layers of adjacent patches. Ply shares are constrained between 10–63% for  $0^\circ$  and  $90^\circ$  fibres and 20–80% for  $\pm 45^\circ$  fibres. Additionally, the wing tip twist is constrained to  $-6.76^\circ$  for F25-AR15 and  $-7.01^\circ$  for F25-AR17, based on an extrapolation of the A320neo's twist [15], with a 1.5 safety factor applied.

## 5. RESULTS

In this section, the results of the structural sizing and performance prediction of both F25-AR15 and F25-AR17 aircraft models are presented.

### 5.1. Structural Sizing

Prior to the optimisation, both F25-AR15 and F25-AR17 had uniform wing properties. Table 3 shows the initial wing structural mass and wing tip displacement under different loading conditions.

	F25-AR15	F25-AR17
Wing Structural Mass [Kg]	4237,63	4502,63
Displ. Cruise - MTOW [m]	2,07	2,78
Displ. Cruise - MZFW [m]	1,80	2,41
Displ. 2.5g - MTOW [m]	5,17	6,94
Displ. 2.5g - MZFW [m]	4,49	6,02

TAB 3. Comparison of wing structural mass and displacements under different load conditions for the pre-sized F25-AR15 and F25-AR17 configurations.

As neither aircraft had been structurally sized, they did not meet the imposed structural safety requirements,

with significant constraint violations, particularly near the wing root. For example, Figure 6 illustrates buckling constraint violations in the upper wing skin.

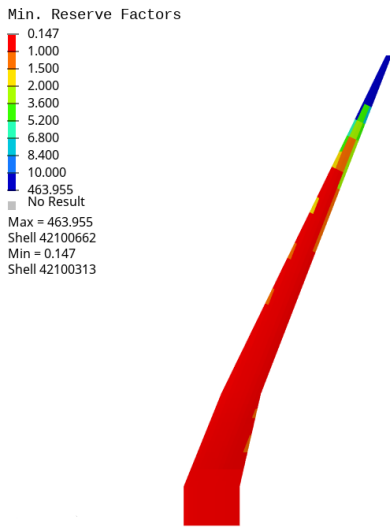


FIG 6. Pre-sized F25-AR15 Upper Skin Buckling Reserve Factors.

As such both models were structurally sized. Table 4 presents the structural mass and displacement of the sized aircraft wing under various load conditions.

	F25-AR15	F25-AR17
Wing Structural Mass [Kg]	5321,99	5615,29
Displ. Cruise - MTOW [m]	1,46	1,91
Displ. Cruise - MZFW [m]	1,27	1,65
Displ. 2.5g - MTOW [m]	3,65	4,78
Displ. 2.5g - MZFW [m]	3,17	4,12

TAB 4. Comparison of wing structural mass and displacements under different load conditions for the sized F25-AR15 and F25-AR17 configurations.

The structural mass of the wing increased by 25.59% for the F25-AR15 and by 24.71% for the F25-AR17, enhancing the wing stiffness, which reduced the maximum wing bending. Although the mass increased compared to the initial models, the sized designs are outcomes of a multidisciplinary optimisation process aimed at finding an optimum that satisfies all constraints, so this mass increase should not be seen negatively. As expected, the F25-AR17 wing, with its increased span and area, exhibits a 5.51% higher structural mass compared to the lower aspect ratio wing.

The sized design for the F25-AR15 shows a markedly different skin thickness distribution compared to the initial model. As shown in Figure 7, the upper skin is thickest in the pylon area, where the loads are highest due to the engine and pylon weight. Towards the wing tip, the skin thickness tapers towards the minimum required 4 mm.

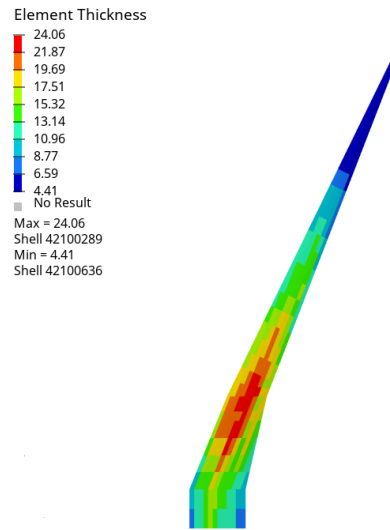


FIG 7. Sized F25-AR15 Upper Skin Thickness Distribution.

For the lower skin, Figure 8, the thickness near the pylon area is at the minimum imposed 20 mm, tapering to 6 mm at the tip and 8 mm at the root. Both upper and lower skins show gradual changes in thickness between patches, as required for manufacturability. The dimension changes for the stringers and spars follow similar trends to the skin.

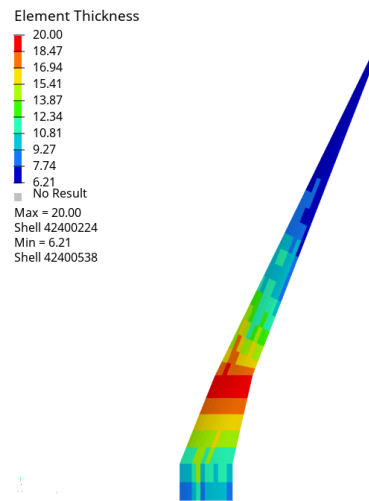


FIG 8. Sized F25-AR15 Lower Skin Thickness Distribution.

Figures 9, 10, and 11 depict the sized wing ply share distribution for the 0°, ±45°, and 90°fibres, respectively. For the upper skin, the ±45°plies concentrate inboard of the pylon and at the wing tip, while the 0°plies are mostly concentrated at the root. In contrast, the 90°plies are sparsely distributed in this area. On the lower skin, ±45°plies are concentrated at the wing tip, while the 0°plies concentrate at the root and along a portion of the leading edge. The 90°plies have their highest concentration at the root. Overall, ±45°and 0°plies maintain the highest ply shares, while the 90°plies become less prevalent.

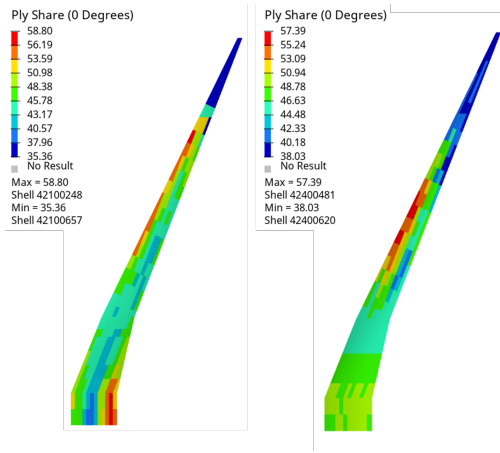


FIG 9. Sized F25-AR15 0° Ply Share Distribution: upper skin (left) and lower skin (right).

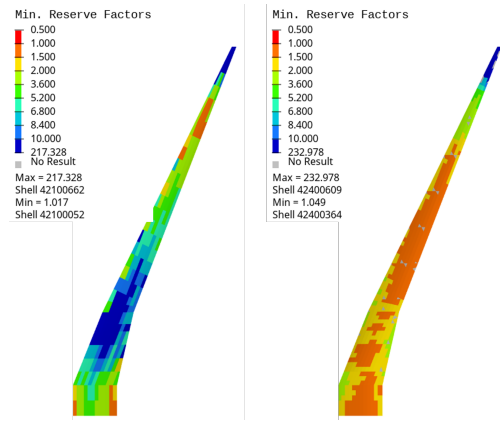


FIG 12. Sized F25-AR15 Reserve Factors: buckling in upper skin (left) and strength in lower skin (right).

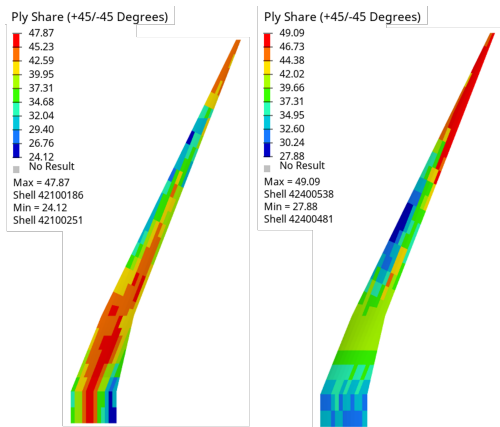


FIG 10. Sized F25-AR15 ±45° Ply Share Distribution: upper skin (left) and lower skin (right).

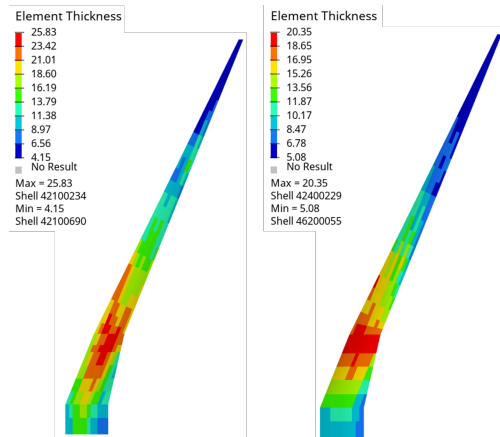


FIG 13. Sized F25-AR17 Upper and Lower Skin Thickness Distribution.

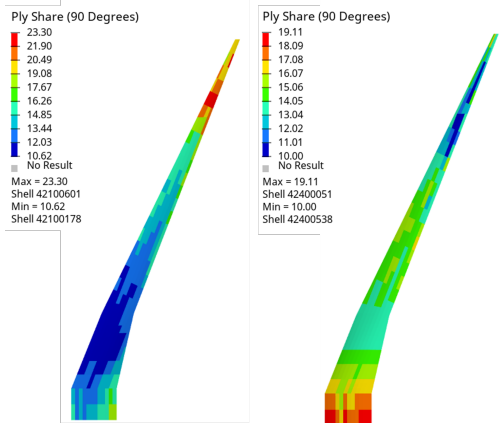


FIG 11. Sized F25-AR15 90° Ply Share Distribution: upper skin (left) and lower skin (right).

Figure 12 shows that, buckling presented the highest reserve factors, particularly near the pylon and wing tip, while strength-related reserve factors are closer to unity, except at the tip. Manufacturing requirements represent the most limiting constraints in the optimisation, with reserve factors close to 1 uniformly across the wing structure, preventing further improvements.

The F25-AR17 showed qualitatively similar results to the F25-AR15 in terms of skin thickness distribution, ply share percentage, spar and stringer sizing, and reserve factor behaviour. Figure 13 depicts the upper and lower skin thickness distribution for the sized F25-AR17, highlighting its resemblance to the F25-AR15 configuration.

For both the upper and lower skins, the higher aspect ratio configuration exhibits a slightly thicker skin in the pylon area. In contrast, the tip of the F25-AR17's wing is less rigid than that of its lower aspect ratio counterpart. This reduced stiffness at the tip, combined with the increased span of the F25-AR17, explains why its wingtip displacements are greater than those of the F25-AR15. Additionally, in the higher aspect ratio model, the proportion of 0° plies has increased slightly, reaching the manufacturing maximum of 63% in some patches near the root and leading edge. Conversely, the 90° plies show a decrease in their ply share compared to the F25-AR15, especially in the lower skin, where they approach the manufacturing minimum of 10%. Even though the reserve factors across the F25-AR17 configuration follow a distribution similar to that of the F25-AR15, their values are slightly lower.

## 5.2. Performance Analysis

To assess the performance of both aircraft models, a 1g load was applied to simulate inertial forces during cruise flight conditions. In the analysis of the lift and drag coefficients for both models, the reference area of the F25-AR15 was used.

From the performance analysis, the in-flight twist was determined, revealing a noticeable washout effect in both wings, as shown in Figure 14. Washout is particularly advantageous, as it helps optimise lift distribution along the span, potentially reducing induced drag, while also preventing wingtip stall. Up to the pylon area, where the wing planform remains constant, the twist distribution for both models is quite similar. Beyond this point, however, the washout effect becomes more pronounced in the higher aspect ratio wing

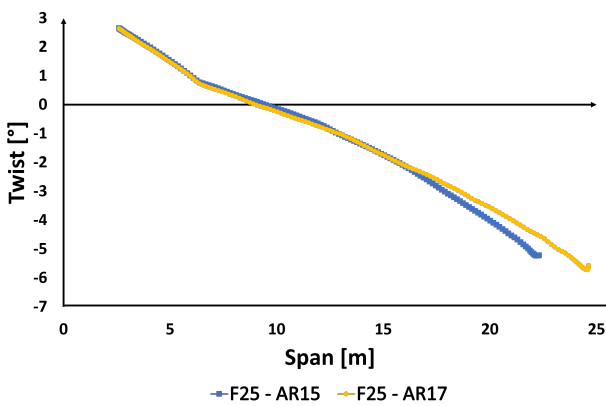


FIG 14. F25-AR15 and F25-AR17 In-Flight Twist Distribution.

In Figure 15, the lift distribution over the normalised span is depicted. The F25-AR15 shows a more elliptical lift distribution, indicating potentially higher aerodynamic efficiency. However, when considering Figure 16, which illustrates the lift distribution over the actual span, it becomes clear that the outboard section of the F25-AR17 generates more lift, suggesting better aerodynamic performance for this model.

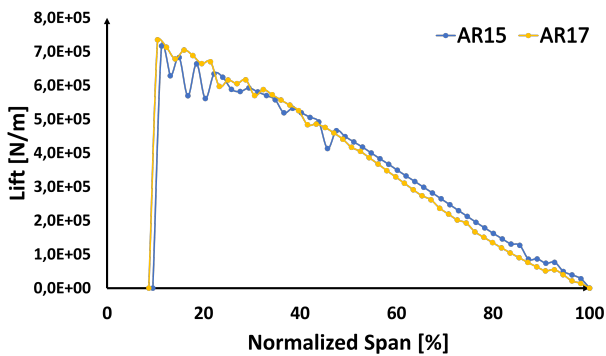


FIG 15. Lift distribution of the F25-AR15 and F25-AR17 models over the normalised span.

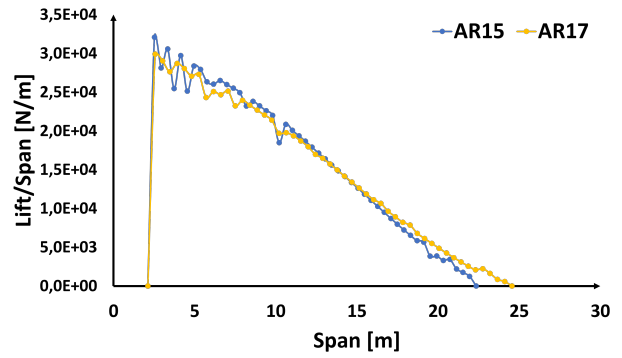


FIG 16. Lift distribution of the F25-AR15 and F25-AR17 models over the actual span.

Table 16 presents the differences in drag counts between the F25-AR17 and F25-AR15 models. As expected, the F25-AR17 shows an increase of 10.1% in friction drag due to its larger wing surface area. However, the increased span results in a 6.64% reduction in the wing's induced drag. Additionally, as the F25-AR17 generates more lift, it requires a lower angle of attack, thereby reducing the pressure drag generated by the fuselage. Overall, the F25-AR17 achieves greater lift and reduces total drag, thereby improving aerodynamic performance.

Drag Counts			
	Pressure	Friction	Total
Wing	-6,409	4,447	-1,962
Fuselage	-2,739	0,028	-2,711
<b>Total</b>	<b>-9,148</b>	<b>4,475</b>	<b>-4,673</b>

TAB 5. Difference of drag counts between the F25-AR17 and F25-AR15 models

To compare the range of both aircraft, it was assumed that the thrust-specific fuel consumption was the same in both models, and that the available fuel for the F25-AR15's mission was the difference between its MTOW and MZFW. As both aircraft were designed for the same MTOW, but the F25-AR17 has a higher structural mass, it was simplistically assumed that the F25-AR17 would carry less fuel, with the reduction equal to the increase in structural mass. Under these assumptions, the F25-AR17 demonstrated a 1.47% increase in the Breguet range.

## 6. CONCLUSIONS AND FUTURE WORK

In this study, two aircraft, based on the DLR F25 model and with high aspect ratios of 15.5 and 17.4, were structurally sized using the MDO suite Lagrange. Afterwards their performance was assessed using high-fidelity analysis methods, including TAU within FlowSimulator. Structural sizing was performed using gradient-based methods, considering sizing parameters for the composite wing covers and spars under strength, buckling, and manufacturing constraints to reflect industry requirements. The results from the structural sizing of both aspect ratios showed qualitatively similar trends in skin

thickness distribution, ply share allocation, and spar and stringer sizing. However, the higher aspect ratio aircraft exhibited lower reserve factors. It was evident that, in both cases, strength and manufacturing constraints were the most challenging to satisfy. Furthermore, the minimum thickness requirements limited the potential for weight savings, particularly near the wing tip and, in the case of the lower skin, around the pylon area. Upon completion of the structural sizing, a performance prediction was carried out using the high-fidelity MDO framework. The aircraft with the higher aspect ratio demonstrated superior aerodynamic performance and an estimated increase of 1.47% in Breguet range. Future work should aim to improve the aerodynamic fidelity within the structural sizing process, and explore high-fidelity MDO optimisations for performance considering shape and sizing variables simultaneously, to further refining the design space exploration.

## ACKNOWLEDGEMENTS & DISCLAIMERS

The project Ultra Performance Wing (UP Wing, project number: 101101974) is supported by the Clean Aviation Joint Undertaking and its members. Co-Funded by the European Union. Views and opinions expressed are however those of the author(s) only and do not necessarily reflect those of the European Union or Clean Aviation Joint Undertaking. Neither the European Union nor the granting authority can be held responsible for them.

### Contact address:

[luis\\_miguel.martins\\_pacheco@airbus.com](mailto:luis_miguel.martins_pacheco@airbus.com)

## References

- [1] G. Schuhmacher, F. Daoud, Ö. Petersson and M. Wagner. Multidisciplinary airframe design optimization. In *28th International Congress of the Aeronautical Sciences*. ICAS, Brisbane, Australia, 23 - 28 September 2012.
- [2] L. Reimer. The FlowSimulator - A Software Framework for CFD-related Multidisciplinary Simulations. In *European NAFEMS Conference Computational Fluid Dynamics (CFD) - Beyond the Solve*. Munich, Germany, 2 - 5 December 2015.
- [3] P. M. Weaver. On Optimisation of Long Anisotropic Flat Plates Subject to Shear Buckling Loads. In *45th AIAA/ASME/ASCE/AHS/ASC Structures, Structural Dynamics Materials Conference*. Palm Springs, California, 19 - 22 April 2004.
- [4] P. M. Weaver. Design Formulae for Buckling of Biaxially Loaded Laminated Rectangular Plates with Flexural/twist Anisotropy. In *46th AIAA/ASME/ASCE/AHS/ASC Structures, Structural Dynamics and Materials Conference*. Austin, Texas, 18 - 21 April 2005.
- [5] D. E. Calderon, J. E. Cooper, M. Lowenberg, S. A. Neild and E. B. Coetzee. Sizing High-Aspect-Ratio Wings with a Geometrically Nonlinear Beam Model. *Journal of Aircraft*, 56:1455–1470, 2019. DOI: [10.2514/1.C035296](https://doi.org/10.2514/1.C035296).
- [6] F. Volle, M. Abu-Zuray, A. Balani, U. Anjali, S. Deinert, Ö. Petersson. Simultaneous Shape and Sizing Optimization for Improving Aircraft Performance Using the Adjoint Approach. In *DLRK Conference*. Stuttgart, Germany, 19 - 21 September 2023.
- [7] A. A. Gastaldi, F. Volle, F. Daoud, and C. Breitsamter. Simultaneous Airframe Shape and Sizing Optimization using FlowSimulator and the Lagrange MDO suite. In *DLRK Conference*. Dresden, Germany, 27 - 29 September 2022.
- [8] H. von Geyr A. Krumbein H. Lüdeke D. Schwamborn, A. Gardner and A. Stürmer. Development of the TAU-Code for aerospace applications. In *50th NAL International Conference on Aerospace Science and Technology*. Bangalore, India, 26 - 28 June 2008.
- [9] A. Schwöppe S. Langer and N. Kroll. The DLR Flow Solver TAU - Status and Recent Algorithmic Developments. In *52nd Aerospace Sciences Meeting*. Maryland, USA, 13 - 17 January 2014.
- [10] A. Schuster, L. Reimer and J. Neumann. A Mesh-Free Parallel Moving Least-Squares-based Interpolation Method for the Application in Aeroelastic Simulations With the Flow Simulator. *New Results in Numerical and Experimental Fluid Mechanics X*, 132:573–583, 2016. DOI: [10.1007/978-3-319-27279-5\\_50](https://doi.org/10.1007/978-3-319-27279-5_50).
- [11] A. Rempke. Netzdeformation mit Elastizitätsanalogie in multidisziplinärer FlowSimulator-Umgebung. In *Jahresbericht 2016 zum 20. DGLR-Fach-Symposium der STAB*. Braunschweig, Germany, 9 - 10 November 2016.
- [12] R. Maierl, Ö. Petersson, F. Daoud. Automated Creation of Aeroelastic Optimization Models from a Parameterized Geometry. In *15th International Forum on Aeroelasticity and Structural Dynamics*, 2013.
- [13] K. Schittkowski. NLPQL: A fortran subroutine solving constrained nonlinear programming problems. *Annals of Operations Research*, 5:485–500, 1986. DOI: [10.1007/BF02022087](https://doi.org/10.1007/BF02022087).
- [14] S. Boyd and L. Vandenberghe. *Convex optimization*. Cambridge university press, 2004.
- [15] M. Orlita and R. Vos. Cruise Performance Optimization of the Airbus A320 through Flap Morphing. In *17th AIAA Aviation Technology, Integration, and Operations Conference*. Denver, Colorado, 5 - 9 June 2017.